# Improved nucleation of TiN atomic layer deposition films on SiLK* low-*k* polymer dielectric using an $Al_2O_3$ atomic layer deposition adhesion layer

J. W. Elam, C. A. Wilson, M. Schuisky, Z. A. Sechrist, and S. M. George[a)]
*Department of Chemistry and Biochemistry, University of Colorado, Boulder, Colorado 80309-0215*

(Received 10 June 2002; accepted 4 April 2003)

Diffusion barriers are required to prevent copper from diffusing into low-*k* polymer dielectrics in backend interconnects. The ability to deposit conformal diffusion barriers onto high aspect ratio, low-*k* polymer features requires atomic layer deposition (ALD) techniques. This study examined TiN ALD on SiLK (a trademark of the Dow Chemical Company) low-*k* polymer dielectric using tetrakis-dimethylamino titanium and $NH_3$. X-ray fluorescence spectroscopy (XRFS), optical microscopy, and surface profiling of the TiN ALD films deposited on SiLK revealed discontinuous films displaying distinct patchy regions. The patches corresponded to a thinner TiN coating and were attributed to difficulties for TiN ALD nucleation on SiLK. To study TiN ALD nucleation, *in situ* quartz-crystal microbalance (QCM) measurements were performed by spincoating SiLK onto the QCM sensor. Subsequent QCM measurements during TiN ALD revealed very low initial TiN ALD growth rates indicating poor nucleation. $Al_2O_3$ ALD was then performed on the SiLK film using trimethyl aluminum and $H_2O$. Surface profiling, XRFS, QCM, and transmission electron microscopy measurements revealed that the $Al_2O_3$ ALD film nucleates immediately on SiLK producing a continuous $Al_2O_3$ film. In addition, QCM measurements showed that TiN ALD nucleates readily on the $Al_2O_3$ surface. The $Al_2O_3$ ALD adhesion layer facilitated the growth of a continuous TiN ALD film on SiLK. Examination of TiN ALD films prepared on SiLK with progressively thinner $Al_2O_3$ ALD adhesion layers revealed that 10 $Al_2O_3$ ALD cycles were sufficient to promote the nucleation of the TiN ALD film. © *2003 American Vacuum Society.*
[DOI: 10.1116/1.1577568]

PROOF COPY 039303JVB

## I. INTRODUCTION

Previous semiconductor devices have employed aluminum alloy interconnects insulated by $SiO_2$ dielectric layers. As semiconductor devices are fabricated with smaller dimensions, the resistance capacitance (RC) time constant of the interconnects eventually limits the device speed.[1] One strategy for reducing the RC time constant is to change the interconnect conductor from the aluminum alloy with a resistivity of $\rho = 2.66\ \mu\Omega$ cm to copper with a resistivity of $\rho = 1.67\ \mu\Omega$ cm.[2] This change reduces the RC time constant by ~40%. Further improvements in device performance are achieved by reducing the capacitance of the dielectric volume between the interconnect lines. This reduction may be accomplished by changing from $SiO_2$ with a dielectric constant of $k \sim 4$ to a lower dielectric constant material.[3] Materials with a dielectric constant <4.0 are referred to as "low-*k*" dielectrics.

Many low-*k* organic polymers are being considered to replace $SiO_2$ as the interconnect dielectric.[4] One promising candidate is SiLK, an organic polymer with a dielectric constant of $k = 2.65$ manufactured by the Dow Chemical Company.[5,6] One potential problem with the low-*k* polymer materials is Cu diffusion.[7–10] The migration of Cu atoms from the copper interconnects through the low-*k* polymer at high temperatures in the presence of electric fields can cause device failure.[8] To alleviate this problem, diffusion barrier materials such as TiN may be deposited on the low-*k* dielectric prior to the copper deposition.[10,11] The diffusion barrier layers must be thin to maintain a sufficient interconnect diameter. In addition, the diffusion barrier layer should also be conformal to ensure a uniform coating on the high aspect ratio low-*k* polymer features.

Atomic layer deposition (ALD) is a useful technique for depositing thin conformal films on high aspect ratio structures. ALD utilizes two sequential self-limiting reactions that occur between a gaseous precursor and the solid substrate. By repeating these surface reactions in an ABAB...binary sequence, a thin film can be deposited with atomic layer thickness control.[12,13] ALD methods exist for depositing TiN barrier layers.[14–21] However, only very recent studies have explored the nucleation of TiN ALD films on low-*k* substrates.[11]

This investigation explored the ALD of TiN on SiLK low-*k* polymer films. An $Al_2O_3$ ALD adhesion layer was used to improve the nucleation of the ALD TiN on SiLK. The nucleation and growth of the ALD TiN films on SiLK were studied both with and without the intermediate $Al_2O_3$ ALD adhesion layer. *Ex situ* profilometry, x-ray fluorescence measurements and transmission electron microscopy (TEM) techniques were used to investigate the growth of the TiN and $Al_2O_3$ ALD films. Additionally, *in situ* quartz-crystal microbalance (QCM) techniques were employed to explore the TiN and $Al_2O_3$ ALD nucleation processes.

[a)]Also at Department of Chemical Engineering, University of Colorado, Boulder, CO 80309-0215; electronic mail: steven.george@colorado.edu

PROOF COPY 039303JVB


## II. EXPERIMENT

### A. Viscous flow reactor for atomic layer deposition

The TiN and $Al_2O_3$ ALD films were deposited using a viscous flow ALD reactor that has been described previously.[22] Briefly, the flow reactor consists of a stainless-steel tube with an inside diameter of 3.5 cm. Ultrahigh-purity nitrogen continuously passes through the flow tube at a mass flow rate of ~200 sccm. A gas velocity of ~2.5 m/s and a steady-state pressure of ~1 Torr are maintained in the reactor flow tube using a mechanical pump with a pumping speed of 3.2 l/s. Particulate hydrocarbon and oxygen-containing impurities in the nitrogen carrier gas are reduced to sub-ppb levels using an Aeronex Gate Keeper inert gas filter. The reactor temperature was maintained at 177 °C using a Eurotherm temperature controller.

The ALD flow reactor was equipped with four reactant channels to facilitate the rapid switching between the TiN and $Al_2O_3$ ALD precursors. The TiN ALD was performed using alternating exposures to tetrakis-dimethylamino titanium (TDMAT) and ammonia ($NH_3$).[19,21] TiN ALD using TDMAT and $NH_3$ is believed to proceed according to the following binary reaction sequence:[21]

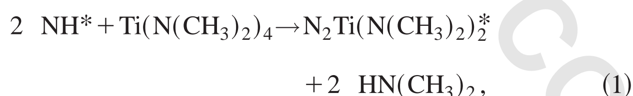

$$2\ \mathrm{NH}^* + \mathrm{Ti(N(CH_3)_2)_4} \rightarrow \mathrm{N_2Ti(N(CH_3)_2)_2^*} + 2\ \mathrm{HN(CH_3)_2}, \quad (1)$$

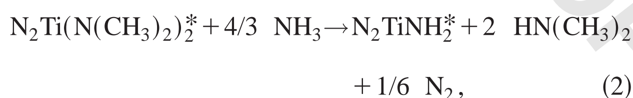

$$\mathrm{N_2Ti(N(CH_3)_2)_2^*} + 4/3\ \mathrm{NH_3} \rightarrow \mathrm{N_2TiNH_2^*} + 2\ \mathrm{HN(CH_3)_2} + 1/6\ \mathrm{N_2}, \quad (2)$$

where the asterisks designate the surface species. Equations (1) and (2) are transamination exchange reactions in which the $NH_x^*$ surface species are replaced by $Ti(N(CH_3)_2)_y^*$ surface species and vice versa. The Ti changes its oxidation number from 4 to 3 in Eq. 2. This change is necessary to achieve the correct Ti oxidation number in bulk TiN.

The TDMAT (Schumacher electronic grade, >99.999%) was held in a stainless-steel bubbler heated to ~50 °C. Ultrahigh-purity nitrogen gas flowed continuously through the bubbler at a mass flow rate of 100 sccm. Computer-controlled pneumatic diaphragm valves directed this flow into the flow reactor during the TDMAT exposures or into a separate mechanical pump during the TDMAT purge times or $NH_3$ exposure and purge times. The $NH_3$ (Aldrich anhydrous, >99.99%,) was delivered using a mass flow controller operating at 600 sccm. Computer-controlled valves directed this 600 sccm $NH_3$ flow into the viscous flow reactor during the $NH_3$ exposures or into a mechanical pump during the $NH_3$ purge times or the TDMAT exposure and purge times. The TiN ALD pulse sequence was: 1 s TDMAT exposure; 0.5 s TDMAT purge; 1 s $NH_3$ exposure; and 5 s $NH_3$ purge. These conditions yield a TiN ALD growth rate at 177 °C of 1.6 Å/cycle.[21]

The $Al_2O_3$ ALD was accomplished using alternating exposures to trimethyl aluminum (TMA) and $H_2O$.[23–25] $Al_2O_3$ ALD proceeds according to the following binary reaction sequence:[24,25]

$$\mathrm{AlOH}^* + \mathrm{Al(CH_3)_3} \rightarrow \mathrm{AlOAl(CH_3)_2^*} + \mathrm{CH_4}, \quad (3)$$

$$\mathrm{AlCH_3^*} + \mathrm{H_2O} \rightarrow \mathrm{AlOH}^* + \mathrm{CH_4}. \quad (4)$$

The semiconductor grade TMA with a purity of 99.9999% was obtained from Akzo Nobel. The Optima purity deionized $H_2O$ was obtained from Fisher. The $Al_2O_3$ ALD pulse sequence used 1 s reactant exposures and 5 s purges between the reactant exposures. These conditions yield an $Al_2O_3$ ALD growth rate of 1.29 Å/cycle.[26]

The viscous flow ALD reactor was equipped with an *in situ* QCM.[22] Polished QCM sensors from Colorado Crystal Corporation (Part No. CCAT1BK-1007-000) were mounted in a Maxtek BSH-150 bakeable sensor head attached to a 2.75 in. Conflat flange. The sensor head was modified to provide an ~20 sccm nitrogen flow over the back surface of the sensor crystal to prevent deposition on the back side of the sensor. Signals from the QCM sensor were measured by a Maxtek TM400 film thickness monitor interfaced to a computer. The thickness monitor and interface allow mass measurements with 0.375 ng/cm$^2$ resolution to be performed every 0.1 s. Assuming a TiN density of 5.22 g/cm$^3$, this mass resolution equates to a thickness resolution for TiN of 0.007 Å.

The QCM was employed to investigate the nucleation and growth of the TiN and $Al_2O_3$ films on SiLK. To prepare the SiLK substrate, SiLK J-590 resin was spincoated onto a polished QCM sensor. This spin coating was performed using a rotational speed of 5000 rpm for 60 s. After spincoating, the SiLK was cured in a tube furnace at 400 °C for 60 min under an ultrahigh-purity nitrogen flow of 500 sccm. Surface profiling of the spincoated SiLK films was performed using a Dektak 3 surface profilometer. These measurements obtained a film thickness of ~0.5 $\mu$m on the QCM sensor following the curing procedure. The coated sensor was then installed in the QCM sensor head and loaded into the viscous flow ALD reactor.

### B. Atomic layer deposition film growth and *ex situ* measurements

The TiN and $Al_2O_3$ ALD films were deposited on both Si(100) and SiLK substrates. Prior to deposition, the Si(100) substrates were degreased using a 15 min dip in a piranha solution containing 70 mL $H_2SO_4$ and 30 mL 30% $H_2O_2$ in $H_2O$. The SiLK substrates were prepared by spincoating SiLK J-590 resin onto a Si(100) wafer. The SiLK films were then cured at 400 °C for 60 min. These SiLK films on Si(100) had a thickness of ~1.8 $\mu$m.

Thickness measurements were performed on the $Al_2O_3$ ALD films deposited on SiLK using the Dektak 3 surface profilometer. Steps were created in the $Al_2O_3$ films by masking a portion of the surface using a high-temperature aluminum foil tape (3M 433) prior to loading the samples into the flow reactor. The relative thicknesses of the TiN films deposited on the SiLK substrates were determined from x-ray fluorescence spectroscopy (XRFS) measurements using a


PROOF COPY 039303JVB

PROOF COPY 039303JVB


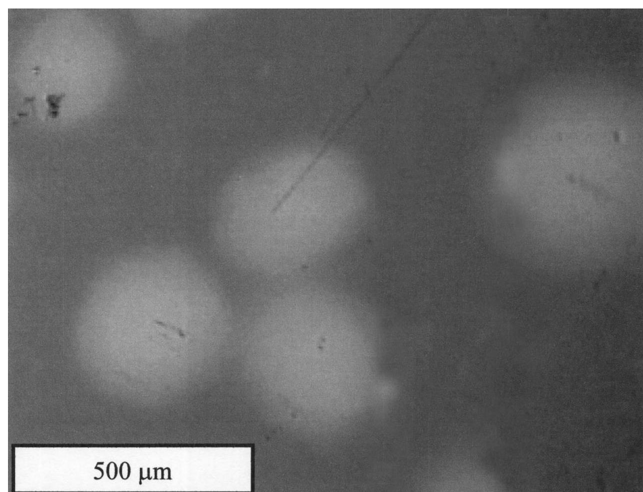


FIG. 1. Optical micrograph of a TiN ALD film deposited on a SiLK substrate showing distinct patches surrounded by uniform regions.

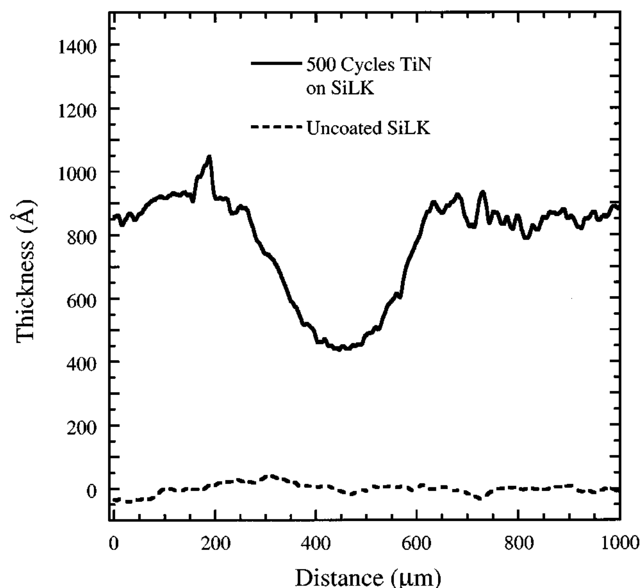


FIG. 2. Surface profilometer scans across a distinct patch in a TiN ALD film deposited on a SiLK substrate (solid line) and across an uncoated SiLK substrate (dashed line).

Spectro X-lab 2000 spectrometer at the Department of Materials Chemistry in the Ångström Laboratory at Uppsala University.

The $Al_2O_3$ ALD films on the SiLK substrates were characterized using TEM and energy dispersive spectroscopy (EDS) of cross-sectional specimens. The cross-sectional TEM specimen was prepared by gluing two pieces of the thin-film sample face to face. A cross-sectional sample was cut and mechanically ground on both sides to a thickness of 100 $\mu$m. The sample was dimpled down to a thickness of 10 $\mu$m at the specimen center and ion milled until the center region was electron transparent.

The TEM measurements employed a JEOL 2000 FXII operating at 200 kV and a TECNAI F30 ST field-emission gun operated at 300 kV with a Gatan Imaging Filter. An EDAX energy dispersive x-ray spectroscopy system was used to study the elemental composition of the specimens. The TEM and EDS measurements were performed by Dr. Jun Lu at the Department of Materials Chemistry in the Ångström Laboratory at Uppsala University.

## III. RESULTS

### A. TiN atomic layer deposition on SiLK

TiN ALD films were deposited onto SiLK substrates using 500 AB cycles of TDMAT and $NH_3$ at 177 °C. These deposition conditions yield uniform TiN films with a thickness of 800 Å when deposited onto Si(100) substrates.[21] Visual inspection of the resulting TiN films deposited on SiLK revealed that the TiN films were composed of uniform regions and distinct patches. Figure 1 shows an optical micrograph of the TiN ALD film deposited on SiLK. The lighter shaded circular regions visible in Fig. 1 are the distinct patchy regions.

A surface profilometer scan through one of the distinct patches in the TiN ALD film is shown by the solid line in Fig. 2. These data have been offset in order that the regions of the TiN film outside of the distinct patch have a thickness of 800 Å. The solid line in Fig. 2 indicates that the distinct patches in the TiN film are only about one half of the thickness of the uniform regions of the TiN film. For comparison, the dashed line in Fig. 2 is a surface profilometer scan of a SiLK film with no TiN ALD.

The TiN ALD films deposited on SiLK were also investigated using XRFS measurements. The solid circles in Fig. 3 show the Ti XRFS signals recorded from the uniform regions of the TiN films following 25, 50, 100, 200, 350, and 500 AB cycles. In contrast, the open squares in Fig. 3 present the Ti

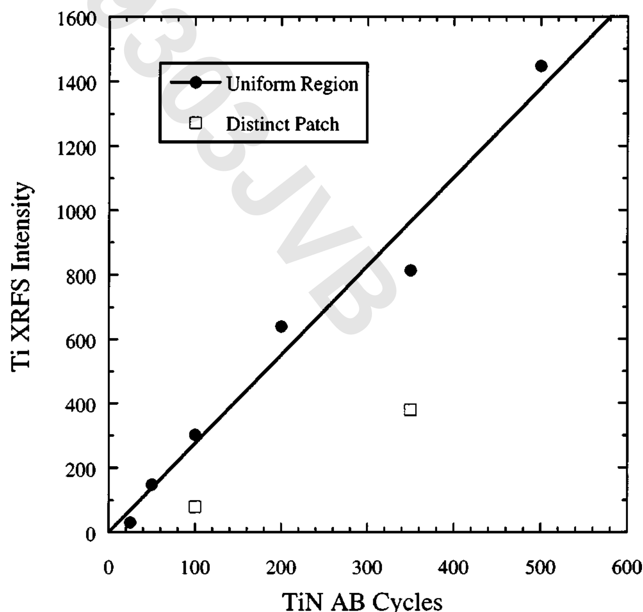


FIG. 3. Ti XRFS intensity from TiN ALD films deposited on SiLK substrates vs TiN AB cycles. The solid circles were recorded from uniform regions of the TiN film. The open squares were recorded from the distinct patches.


PROOF COPY 039303JVB

PROOF COPY 039303JVB


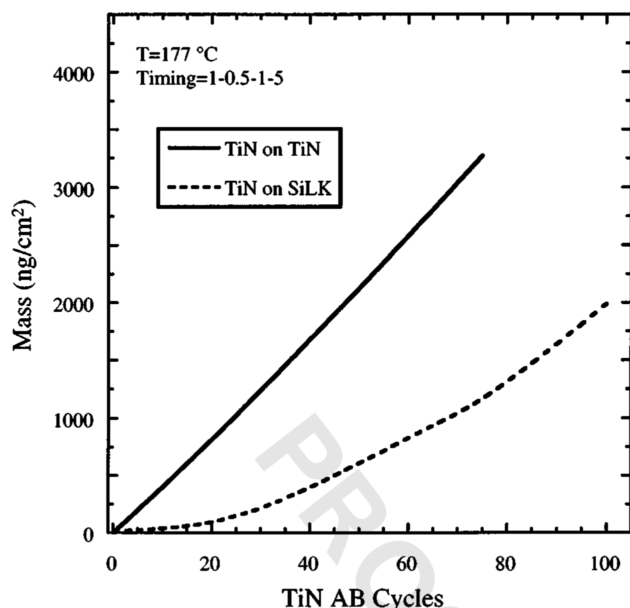


FIG. 4. Mass measured by the in situ QCM vs TiN AB cycles on SiLK (dashed line) and on TiN (solid line).

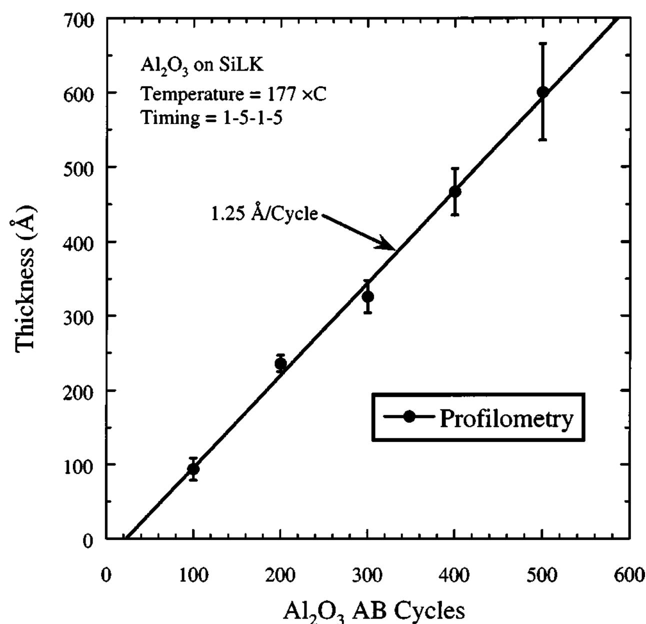


FIG. 5. Thickness measured using the surface profilometer vs $Al_2O_3$ AB cycles on SiLK substrates.

XRFS signals measured from the distinct patches visible on the samples prepared using 100 and 350 AB cycles. Figure 3 demonstrates that the distinct patches have a lower coverage of Ti atoms.

*In situ* QCM measurements were performed to explore the initial nucleation of the TiN ALD on SiLK. SiLK was deposited onto a QCM sensor by spincoating. The dashed line in Fig. 4 shows the QCM measurements recorded during the TiN ALD on SiLK. Figure 4 reveals that the TiN ALD growth is initially very low on SiLK. The average TiN ALD growth rate during the first 10 cycles is only 3.7 $ng/cm^2$/cycle. Following 75 TiN ALD cycles on SiLK, the TiN growth rate is 27 $ng/cm^2$/cycle and the accumulated mass change is 1170 $ng/cm^2$.

For comparison, the solid line in Fig. 4 shows the QCM measurements resulting from 75 TiN AB cycles on a TiN surface. This TiN surface was prepared by performing several hundred TiN AB cycles. After this procedure, the TiN ALD achieves a steady-state growth rate of 44 $ng/cm^2$/cycle and yields a mass change of 3275 $ng/cm^2$ for 75 AB cycles.

### B. $Al_2O_3$ atomic layer deposition on SiLK

$Al_2O_3$ ALD films were deposited on SiLK substrates using 100, 200, 300, 400, and 500 AB cycles. Visual inspection of the $Al_2O_3$ ALD films indicated that they were highly uniform. Figure 5 presents the surface profilometer thickness measurements for these films. A linear least-squares fit to the data in Fig. 5 yields an $Al_2O_3$ ALD growth rate of 1.25 Å/cycle. The least-squares fit intersects the $x$ axis in Fig. 5 at $23\pm 12$ AB cycles. This $x$-axis intersection may suggest a nucleation period of inhibited $Al_2O_3$ growth on SiLK for the first ~23 AB cycles.

The $Al_2O_3$ ALD films on the SiLK substrates were also analyzed using XRFS techniques. The solid circles in Fig. 6 plot the relative Al XRFS signals resulting from the $Al_2O_3$ ALD films deposited on the SiLK substrates. In contrast to the surface profilometer results, the Al XRFS signals suggest that the $Al_2O_3$ ALD growth rate is larger initially and then reaches a constant value following ~25 AB cycles. This difference is very interesting and provides information about the initial growth of $Al_2O_3$ ALD on SiLK.

*In situ* QCM measurements were also performed to measure the nucleation and growth of the $Al_2O_3$ ALD films on SiLK. The solid line in Fig. 6 shows the QCM measurements obtained for $Al_2O_3$ ALD on SiLK. The vertical axis for mass and Al XRFS intensity have been adjusted to show the proportionality between these two signals. Figure 6 demon-

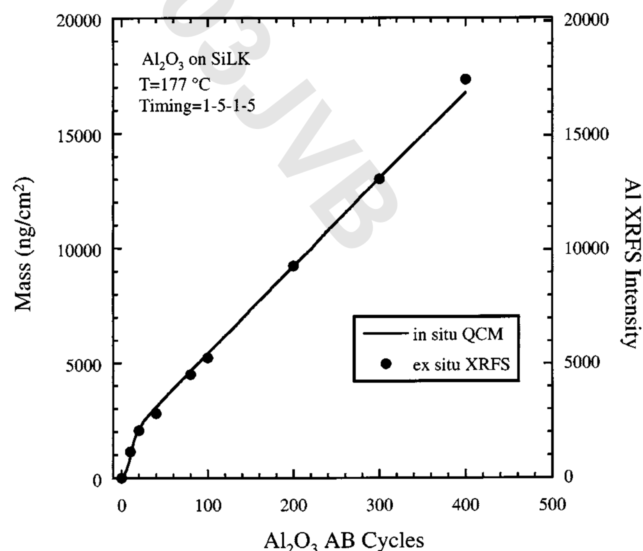


FIG. 6. Mass measured by the *in situ* QCM (solid line) and *ex situ* Al XRFS intensity (solid circles) versus $Al_2O_3$ AB cycles on SiLK substrates.


PROOF COPY 039303JVB

PROOF COPY 039303JVB


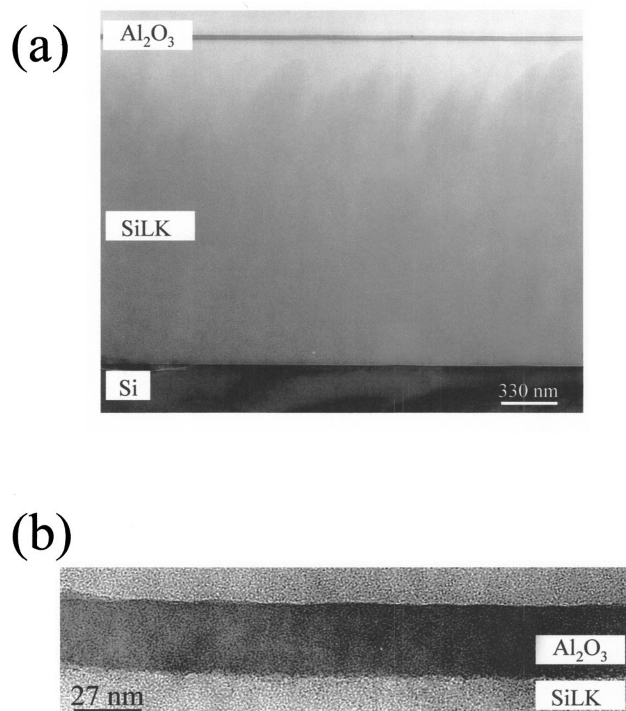


FIG. 7. Cross-sectional TEM images of an $Al_2O_3$ ALD film deposited on a SiLK substrate at (a) low and (b) high magnification.

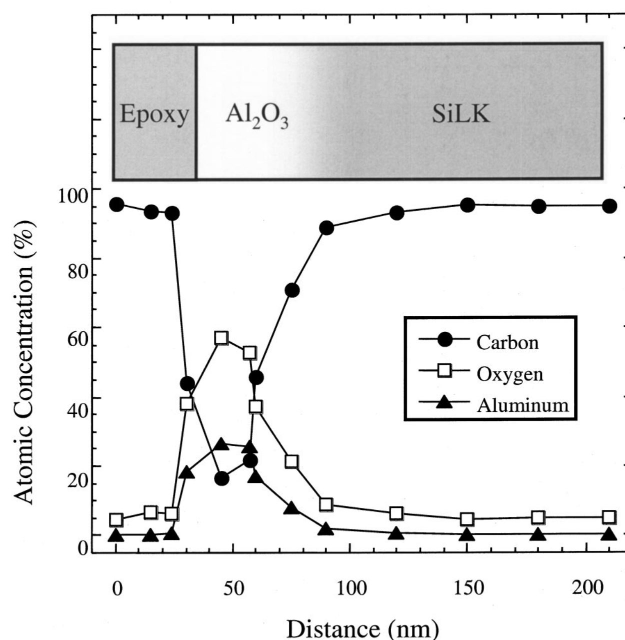


FIG. 8. Cross-sectional EDS scan of the interface between an $Al_2O_3$ ALD film and the underlying SiLK layer showing the spatial variation of the C, O, and Al atomic concentrations.

COPY 039303JVB

strates that the QCM measurements and the XRFS measurements correspond to each other very well. The QCM measurements show an enhanced $Al_2O_3$ ALD growth rate for the first ~25 AB cycles. After this nucleation period, the $Al_2O_3$ growth decreases and attains a steady-state growth rate of 38 ng/cm$^2$/cycle.

TEM analysis was performed on the $Al_2O_3$ ALD film deposited on the SiLK substrate using 200 AB cycles. The bright-field TEM image shown in Fig. 7(a) clearly shows the $Al_2O_3$ ALD film, the SiLK layer and the underlying Si(100) substrate. The $Al_2O_3$ ALD film appears to be very uniform and smooth. The higher-resolution TEM image shown in Fig. 7(b) reveals that the interface between the $Al_2O_3$ ALD film and the SiLK layer is relatively sharp. The $Al_2O_3$ ALD film thickness measured from Fig. 7(b) is ~30 nm. This thickness is greater than both the thickness of ~23 nm determined by the surface profilometer measurements in Fig. 5 and the predicted thickness of 25 nm from the $Al_2O_3$ ALD growth rate of 1.25 Å/cycle.

Figure 8 shows the EDS profile of the interface between the $Al_2O_3$ ALD film and the SiLK layer. The solid circles, open squares, and solid triangles in Fig. 8 plot the percentage atomic concentrations for carbon, oxygen, and aluminum, respectively. The interface between the overlying epoxy and the $Al_2O_3$ ALD film occurs at ~30 nm. This interface is characterized by a drop in the carbon concentration that is coincident with an increase in the oxygen and aluminum concentrations. The EDS resolution is estimated to be ~15 nm based on the EDS profile across this epoxy/$Al_2O_3$ interface.

The $Al_2O_3$ region of Fig. 8 has a full width at half maximum of ~32 nm. This value is slightly larger than the thickness of ~30 nm determined from Fig. 7(b) and also larger than the thickness of 25 nm predicted from the $Al_2O_3$ ALD growth rate. The larger $Al_2O_3$ ALD thickness determined from the EDS measurements may result from diffusion of the TMA and $H_2O$ precursors into the SiLK. In agreement with this idea, the slow decrease of the oxygen and aluminum signals versus distance at the $Al_2O_3$/SiLK interface in Fig. 8 suggests a diffuse boundary between these two materials. The transition between $Al_2O_3$ and SiLK occurs over ~35 nm. Assuming an EDS resolution of ~15 nm, the diffuse $Al_2O_3$/SiLK interfacial region has an estimated thickness of ~20 nm.

### C. TiN atomic layer deposition on $Al_2O_3$ atomic layer deposited surfaces

*In situ* QCM measurements were performed to investigate the nucleation and growth of TiN ALD films on the $Al_2O_3$ ALD surface. An $Al_2O_3$ ALD surface was prepared on the QCM sensor by performing 50 TMA/$H_2O$ AB cycles at 177 °C. Following this procedure, TiN ALD was initiated using TDMAT/$NH_3$ AB cycles. The dashed line in Fig. 9 demonstrates that the TiN ALD nucleates immediately on the $Al_2O_3$ surface. During the first cycle of TiN ALD on the $Al_2O_3$ surface, the QCM registers a mass increase of 33 ng/cm$^2$. After 100 AB cycles, the TiN ALD has achieved a growth rate of 39 ng/cm$^2$/cycle. For comparison, the solid line in Fig. 9 shows the QCM measurements for TiN ALD on a TiN surface. The steady-state growth rate measured using the QCM during TiN ALD is 44 ng/cm$^2$/cycle.


PROOF COPY 039303JVB

PROOF COPY 039303JVB


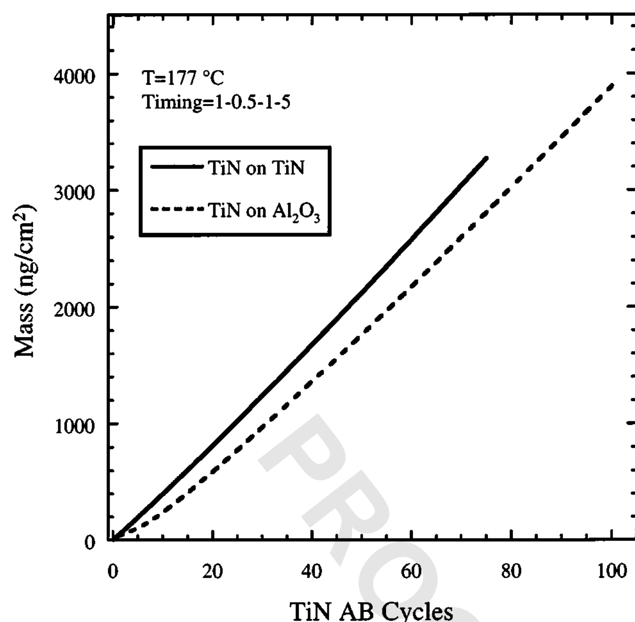


FIG. 9. Mass measured by the *in situ* QCM vs TiN AB cycles on an $Al_2O_3$ ALD surface (dashed line) and a TiN film (solid line).

Additional experiments investigated the influence of an intermediate $Al_2O_3$ ALD adhesion layer on the nucleation of TiN ALD on SiLK. Five TiN ALD films were deposited on SiLK substrates in the viscous flow ALD reactor using 0–20 $Al_2O_3$ AB cycles followed by 100 TiN AB cycles. These films were inspected visually and the number of distinct patches on each 6.5 $cm^2$ sample was counted following deposition. The solid circles in Fig. 10 plot the number of distinct patches observed on the TiN films versus the number of $Al_2O_3$ AB cycles in the intermediate adhesion layer.

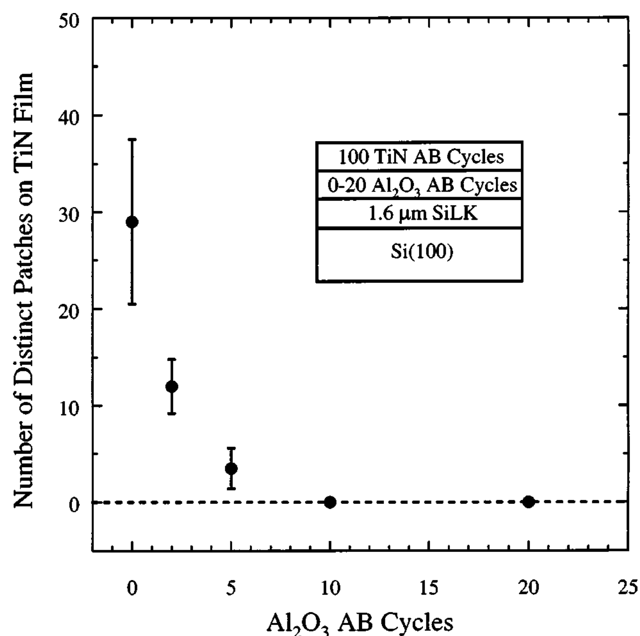


FIG. 10. Number of distinct patches visible on TiN films deposited on SiLK substrates vs $Al_2O_3$ AB cycles used to deposit the $Al_2O_3$ ALD adhesion layer.

Figure 10 demonstrates that the number of distinct patches visible on the TiN ALD films prepared on SiLK decreases dramatically with the number of $Al_2O_3$ AB cycles. The error bars in Fig. 10 represent the standard deviation measured for the number of distinct patches observed on two TiN films prepared under similar conditions. For TiN ALD films prepared using $\geqslant 10$ $Al_2O_3$ AB cycles, no distinct patches were visible on the TiN film surfaces.

## IV. DISCUSSION

### A. TiN atomic layer deposition on SiLK

Figures 1–4 demonstrate that TiN ALD films deposited using TDMAT and $NH_3$ nucleate poorly on SiLK. The TiN ALD films deposited on SiLK are characterized by distinct patches that are thinner and contain less Ti than the surrounding uniform regions. *In situ* QCM measurements reveal that the initial TiN ALD growth rate on SiLK is less than 10% of the steady-state growth rate. Subsequently, the TiN film grows at an increasing rate but does not achieve the steady-state TiN ALD growth rate even after 100 TiN AB cycles.

The QCM measures the average mass change over the entire ~1 $cm^2$ QCM sensor surface. Figure 4 suggests that the TiN ALD does not initially nucleate uniformly over the entire QCM surface. The TiN ALD film begins to grow in more uncoated locations with an increasing number of AB cycles. This interpretation for the TiN nucleation is consistent with the patchy TiN ALD films exhibited in Fig. 1.

The poor nucleation of the TiN ALD films on SiLK probably results from a lack of functional groups to initiate the TiN ALD surface chemistry. The TDMAT is expected to react with amino (NH) or hydroxyl (OH) surface groups to form a Ti—N or Ti—O chemical bond and displace dimethyl amine. In the absence of these groups with nonbonding electron pairs available for nucleophillic attack on the Ti atom in TDMAT, nucleation of TiN ALD is expected to be difficult.

Although the exact composition of SiLK is a trade secret, SiLK is known to be a polyphenylene polymer.[5,6] This polyphenylene polymer is synthesized by reacting cyclopentadienone and acetylene-containing monomers.[6] The aromatic hydrocarbon polymer network of SiLK is comprised of primarily phenyl groups and does not contain nitrogen.[4,27] SiLK does not have $NH^*$ or $Ti(N(CH_3)_2)^*$ surface functional groups to participate in the TiN ALD surface reactions given by Eqs. (1) and (2). Although the SiLK polymer contains oxygen in cyclopentadienone rings, these oxygens are not expected to react with TDMAT.

X-ray photoelectron spectroscopy (XPS) studies of the surface of SiLK polymer have observed a carbon spectrum similar to polystyrene.[28] These XPS investigations also detected a small amount of oxygen in the SiLK substrate. Additional XPS studies explored the surface of SiLK after chemical mechanical polishing (CMP) procedures.[29] These investigations revealed that CMP processing can leave hy-


PROOF COPY 039303JVB

PROOF COPY 039303JVB


droxyl groups on the SiLK polymer surface. The SiLK substrates in the current study were prepared by spincoating and annealing only and were not processed using CMP.

Despite the lack of reactive surface species, the TiN ALD exhibits limited growth on SiLK. The growth of TiN on SiLK may result from the slow thermal decomposition of TDMAT. Alternatively, the growth of TiN could be initiated by the diffusion of the reactants into the SiLK polymer. TDMAT may react with $NH_3$ molecules that have diffused into the SiLK film. Likewise, $NH_3$ may react with TDMAT molecules that have diffused into the SiLK film. These reactions would deposit TiN clusters that would be entangled in the SiLK polymer.

### B. $Al_2O_3$ atomic layer deposited on SiLK

Figure 6 demonstrates that $Al_2O_3$ ALD is facile on SiLK. According to Eqs. (3) and (4), $Al(CH_3)_3$ (TMA) reacts with hydroxyl (OH) groups to deposit aluminum alkyl species on the surface. These $AlCH_3^*$ species then react readily with $H_2O$. This reaction deposits oxygen and rehydroxylates the surface. SiLK does not contain the hydroxyl groups that could react with $Al(CH_3)_3$. Consequently, an alternative mechanism is needed to explain the $Al_2O_3$ ALD on SiLK.

$Al(CH_3)_3$ will probably not react with any chemical moieties in SiLK because TMA is stable in aromatic hydrocarbon solutions such as benzene and toluene. Although SiLK contains oxygen in cyclopentadienone rings in the form of carbonyl groups,[4,6] SiLK that has not been subjected to CMP processing does not have hydroxyl groups to initiate the $Al_2O_3$ ALD chemistry in Eq. (3). The nucleation of $Al_2O_3$ ALD on SiLK requires a mechanism that does not involve the direct reaction between TMA and SiLK.

The nucleation of the $Al_2O_3$ ALD on SiLK may result from the reaction of $H_2O$ with adsorbed TMA in the SiLK polymer. Brunauer–Emmett–Teller measurements indicate that SiLK is very porous with a surface area of 450 $m^2/g$.[10] TMA molecules originating from the TMA ALD exposures may diffuse into the pores in SiLK or be soluble in the SiLK polymer. The subsequent reaction of $H_2O$ with this adsorbed TMA would produce small $Al_2O_3$ clusters entangled in the SiLK polymer with an $AlOH^*$-terminated surface. These surface species would allow the $Al_2O_3$ ALD to proceed by Eqs. (3) and (4).

A second possibility is that $H_2O$ from atmospheric exposure or the $H_2O$ ALD exposures diffuses into the porous SiLK polymer. Although the SiLK polymer is an aromatic hydrocarbon, SiLK does have the capacity to adsorb some moisture. Earlier studies using a 12 $\mu$m thick SiLK film have measured mass increases of 0.08–0.24 wt. % for relative humidities of 20%–80%, respectively.[6] Following the $H_2O$ exposures, the TMA exposure may then react with the $H_2O$ molecules in the near-surface region of the SiLK polymer. This reaction would again produce small $Al_2O_3$ clusters embedded in the polymer network with an $AlCH_3^*$-terminated surface. These surface species would facilitate $Al_2O_3$ ALD according to Eqs. (3) and (4).

The linear least-squares fit to the profilometer data in Fig. 5 suggests that either the $Al_2O_3$ ALD initially grows at a lower rate or that the $Al_2O_3$ ALD requires ~23 AB cycles for nucleation. In contrast, the QCM and XRFS data in Fig. 6 indicate that the $Al_2O_3$ ALD commences immediately and the growth rate is higher for the first ~25 AB cycles. This apparent disagreement may result from the porosity of the SiLK polymer. The surface profilometer measurements may not initially detect the $Al_2O_3$ ALD because the TMA and $H_2O$ may diffuse into the pores of the SiLK polymer. $Al_2O_3$ would then grow in the near-surface region. This $Al_2O_3$ would not deposit on top of the SiLK polymer where the step edge resulting from the deposition could be measured by the surface profilometer.

The QCM and XRFS clearly measure a high initial $Al_2O_3$ ALD growth rate. This high initial growth rate is attributed to the porous SiLK polymer that has a reactant adsorption capacity that is greater than the number of reactive sites on a flat $Al_2O_3$ surface. However, the pores in SiLK will eventually be closed by $Al_2O_3$ ALD. After pore closure, the $Al_2O_3$ growth rates measured by the QCM and XRFS signals should level off and approach the $Al_2O_3$ ALD growth rates measured on a flat surface.

The $Al_2O_3$ ALD growth rates reach their steady-state levels after ~25 AB cycles in Fig. 6. Assuming a growth rate for $Al_2O_3$ of 1.29 Å/cycle,[26] this initial enhanced growth period of ~25 AB cycles suggests that the average pore diameter in SiLK is $d \sim 65$ Å. In agreement with this finding, surface pores were not detected by atomic force microscopy (AFM) measurements on SiLK substrates using an AFM tip with a diameter of $d \sim 200$ Å. The EDS results given in Fig. 8 are also consistent with a porous SiLK polymer. The oxygen and aluminum signals slowly decay over a distance that extends ~20 nm farther into the SiLK polymer than into the epoxy. This slow decay versus distance into the SiLK polymer indicates that the TMA and $H_2O$ precursors can diffuse distances of at least ~20 nm into the pores of the SiLK polymer during the initial $Al_2O_3$ AB cycles.

The $Al_2O_3$/SiLK interface appears sharp in Fig. 7. In contrast, the QCM and XRFS measurements suggest diffusion of the $Al_2O_3$ ALD precursors into the SiLK and the EDS results indicate a diffuse $Al_2O_3$/SiLK boundary. A diffuse $Al_2O_3$/SiLK boundary may be obscured by the contrast conditions used to acquire the TEM images. Although the $Al_2O_3$ ALD growth rate predicts a thickness of only 25 nm, Fig. 7(a) yields an $Al_2O_3$ thickness of 30 nm. Therefore, the dark band representing the $Al_2O_3$ film in Fig. 7(a) may include a diffuse boundary with a thickness of 5 nm.

### C. TiN atomic layer deposition on $Al_2O_3$ atomic layer deposited surfaces

Figure 9 demonstrates that the TiN ALD films nucleate easily on the $Al_2O_3$ ALD surface. The facile nucleation of the TiN ALD films on the $Al_2O_3$ ALD surface may result from the reaction of TDMAT with the surface hydroxyl groups on $Al_2O_3$:


PROOF COPY 039303JVB

PROOF COPY 039303JVB



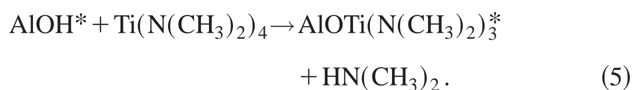

$$AlOH^* + Ti(N(CH_3)_2)_4 \rightarrow AlOTi(N(CH_3)_2)_3^* + HN(CH_3)_2. \quad (5)$$

Although this reaction has not been investigated, the reaction of $Hf(N(CH_3)_2)_4$ with a hydroxylated $HfO_2$ surface is very rapid.[30] The surface hydroxyl groups on $Al_2O_3$ are probably critical for the facile nucleation of the TiN ALD films. An $O_2$ plasma treatment may provide an alternative strategy for depositing surface hydroxyl groups on the low-*k* polymer dielectric surface.[11]

$Al_2O_3$ films can be used as an adhesion layer because $Al_2O_3$ ALD films nucleate well on the SiLK polymer and TiN ALD films nucleate effectively on $Al_2O_3$ ALD films. Figure 10 demonstrates that the $Al_2O_3$ ALD adhesion layer deposited using only 10 AB cycles enhances the TiN ALD nucleation and yields very uniform TiN ALD films. 10 AB cycles should deposit approximately 10–13 Å of $Al_2O_3$. This ultrathin $Al_2O_3$ film thickness should have a minimal effect on the microelectronic device properties.

$Al_2O_3$ ALD films are excellent dielectrics with a dielectric constant of $k \sim 8$.[31] The $Al_2O_3$ ALD adhesion layer may increase the effective dielectric constant of the low-*k* SiLK polymer. However, the thin $Al_2O_3$ ALD layer of only 10–13 Å should have a minimal impact on the dielectric constant. The $Al_2O_3$ ALD adhesion layer may also grow on the copper interconnect lines. Copper is exposed after via formation in the low-*k* dielectric layer during the dual-damascene process. Since $Al_2O_3$ is an insulator, this $Al_2O_3$ ALD layer may increase the resistivity of the conduction line. Fortunately, the $Al_2O_3$ ALD adhesion layer of only 10–13 Å should be thin enough to allow effective electron tunneling.

## V. CONCLUSIONS

TiN ALD films were deposited on SiLK, a low-*k* polymer dielectric, using alternating exposures of TDMAT and $NH_3$. Examination of these films using optical microscopy, surface profilometry, and XRFS techniques established that TiN ALD nucleates poorly on SiLK and produces patchy regions with a nonuniform thickness. *In situ* QCM measurements were performed during TiN ALD on a SiLK film that had been spincoated onto a QCM sensor. These measurements revealed very low initial TiN ALD growth rates suggesting slow, uneven growth of the TiN on SiLK. In contrast, $Al_2O_3$ ALD performed using alternating TMA and $H_2O$ exposures allowed facile $Al_2O_3$ nucleation on SiLK. Because TiN ALD can more readily nucleate on the $Al_2O_3$ ALD film than the SiLK film, an $Al_2O_3$ ALD adhesion layer can improve the nucleation of TiN ALD on SiLK.

Surface profilometry measurements were consistent with ~23 AB cycles required for $Al_2O_3$ ALD nucleation on SiLK. In contrast, *ex situ* XRFS measurements and *in situ* QCM measurements revealed higher initial $Al_2O_3$ ALD growth rates on SiLK. This apparent disagreement was explained by the diffusion of the $Al_2O_3$ ALD precursors into the porous SiLK polymer and the initial growth of $Al_2O_3$ inside the SiLK polymer. In agreement with this finding, EDS measurements indicated that the interface between the $Al_2O_3$ ALD film and the SiLK polymer was relatively diffuse. Examination of TiN ALD films prepared on SiLK substrates with progressively thinner $Al_2O_3$ ALD adhesion layers revealed that 10 $Al_2O_3$ AB cycles were sufficient to promote the nucleation of the TiN ALD films.

## ACKNOWLEDGMENTS

This work was funded by the Semiconductor Research Corporation under a grant from the Intel Corporation. One of the authors (M.S.) acknowledges the Wenner-Gren Foundations and the Sweden–America foundation for financial support. Dr. Jun Lu at the Department of Materials Chemistry in the Ångström Laboratory at Uppsala University performed the TEM and EDS measurements. The XRFS measurements were also performed at the Department of Materials Chemistry in the Ångström Laboratory at Uppsala University.


[1] R. C. Liu, C. S. Pai, and E. Martinez, Solid-State Electron. **43**, 1003 (1999).
[2] Y. Morand, Microelectron. Eng. **50**, 391 (2000).
[3] M. Morgan, E. T. Ryan, J. H. Zhao, C. Hu, T. H. Cho, and P. S. Ho, Annu. Rev. Mater. Sci. **30**, 645 (2000).
[4] G. Maier, Prog. Polym. Sci. **26**, 3 (2001).
[5] P. H. Townsend, S. J. Martin, J. Godschalx, D. R. Romer, J. D. W. Smith, D. Castillo, R. DeVries, G. Buske, N. Rondan, S. Froelicher, J. Marshall, E. O. Shaffer, and J.-H. Im, Mater. Res. Soc. Symp. Proc. **476**, 9 (1997).
[6] S. J. Martin, J. P. Godschalx, M. E. Mills, E. O. Shaffer, and P. H. Townsend, Adv. Mater. (Weinheim, Ger.) **12**, 1769 (2000).
[7] S. A. Cohen, J. Liu, L. Gignac, T. Ivers, D. Armbrust, K. P. Rodbell, and S. M. Gates, Mater. Res. Soc. Symp. Proc. **565**, 189 (1999).
[8] A. L. S. Loke, J. T. Wetzel, P. H. Townsend, T. Tanabe, R. N. Vrtis, M. P. Zussman, D. Kumar, C. Ryu, and S. S. Wong, IEEE Trans. Electron Devices **46**, 2178 (1999).
[9] C. Shim, J. Choi, D. Jung, N.-E. Lee, and C.-W. Yang, Jpn. J. Appl. Phys., Part 2 **39**, L1327 (2000).
[10] J. C. Maisonobe, G. Passemard, C. Lacour, C. Lecornec, P. Motte, P. Noel, and J. Torres, Microelectron. Eng. **50**, 25 (2000).
[11] A. Satta, M. Baklanov, O. Richard, A. Vantomme, H. Bender, T. Conard, K. Maex, W. M. Li, K.-E. Elers, and S. Haukka, Microelectron. Eng. **60**, 59 (2002).
[12] S. M. George, A. W. Ott, and J. W. Klaus, J. Phys. Chem. **100**, 13121 (1996).
[13] M. Ritala and M. Leskela, in *Handbook of Thin-Film Materials*, edited by H. S. Nalwa (Academic, San Diego, 2001).
[14] M. Ritala, M. Leskela, E. Rauhala, and P. Haussalo, J. Electrochem. Soc. **142**, 2731 (1995).
[15] M. Ritala, T. Asikainen, M. Leskela, J. Jokinen, R. Lappalainen, M. Utriainen, L. Niinisto, and E. Ristolainen, Appl. Surf. Sci. **120**, 199 (1997).
[16] M. Ritala, M. Leskela, E. Rauhala, and J. Jokinen, J. Electrochem. Soc. **145**, 2914 (1998).
[17] J.-S. Min, Y.-W. Son, W.-G. Kang, S.-S. Chun, and S.-W. Kang, Jpn. J. Appl. Phys., Part 1 **37**, 4999 (1998).
[18] D.-J. Kim, Y.-B. Jung, M.-B. Lee, Y.-H. Lee, J.-H. Lee, and J.-H. Lee, Thin Solid Films **372**, 276 (2000).
[19] J.-W. Lim, H.-S. Park, and S.-W. Kang, J. Electrochem. Soc. **148**, C403 (2001).
[20] J. Uhm and H. Jeon, Jpn. J. Appl. Phys., Part 1 **40**, 4657 (2001).
[21] J. W. Elam, M. Schuisky, J. D. Ferguson, and S. M. George (unpublished).
[22] J. W. Elam, M. D. Groner, and S. M. George, Rev. Sci. Instrum. **73**, 2981 (2002).
[23] G. S. Higashi and C. G. Fleming, Appl. Phys. Lett. **55**, 1963 (1989).
[24] A. C. Dillon, A. W. Ott, J. D. Way, and S. M. George, Surf. Sci. **322**, 230 (1995).
[25] A. W. Ott, J. W. Klaus, J. M. Johnson, and S. M. George, Thin Solid Films **292**, 135 (1997).


PROOF COPY 039303JVB



PROOF COPY 039303JVB

PROOF COPY 039303JVB


[26]J. W. Elam and S. M. George, Appl. Surf. Sci. (to be published).
[27]J. H. Golden, C. J. Hawker, and P. S. Ho, Semicond. Int. **24**, (2001).
[28]A. Rajagopal, C. Gregoire, J. J. Lemaire, J. J. Pireaux, M. R. Baklanov, S. Vanhaelemeersch, K. Maex, and J. J. Waeterloos, J. Vac. Sci. Technol. B **17**, 2336 (1999).
[29]J. Heeg, U. Schubert, and F. Kuchenmeister, Mikrochim. Acta **133**, 113 (2000).
[30]R. G. Gordon, Chem. Mater. **13**, 2463 (2001).
[31]M. D. Groner, J. W. Elam, F. H. Fabreguette, and S. M. George, Thin Solid Films **413**, 186 (2002).

PROOF COPY 039303JVB


PROOF COPY 039303JVB